THE JOURNAL OF PHYSICAL CHEMISTRY B
A JOURNAL OF THE AMERICAN CHEMICAL SOCIETY

pubs.acs.org/JPCB

Article

Interfacial Dynamics in Lipid Membranes: The Effects of Headgroup Structures

Mason L. Valentine, Maya K. Waterland, Arman Fathizadeh, Ron Elber, and Carlos R. Baiz*

Cite This: *J. Phys. Chem. B* 2021, 125, 1343−1350

Read Online

ACCESS | Metrics & More | Article Recommendations | Supporting Information

ABSTRACT: Phospholipid membranes support essential biochemical processes, yet remain difficult to characterize due to their compositional and structural heterogeneity. The two most common phospholipid headgroup structures in biological membranes are phosphatidylcholine (PC) and phosphatidylethanolamine (PE), but interactions between PC and PE lipids remain underexplored. In this study, we apply ultrafast two-dimensional infrared (2D IR) spectroscopy to quantify the headgroup effects on interfacial dynamics in PC/PE lipid mixtures. Experiments are interpreted through molecular dynamics simulations using the molecular dynamics with alchemical step (MDAS) algorithm for enhanced sampling. Experimental results indicate that the PE content decreases H-bond formation at the ester carbonyl positions near the lipid membrane's hydrophobic core as a result of increased packing density. The observed dehydration is linked to faster molecular dynamics within the interfacial region.

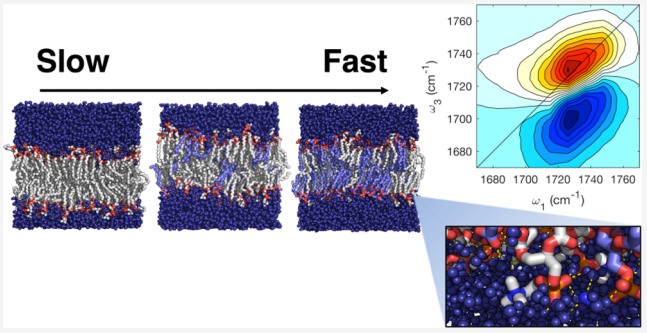

INTRODUCTION

Biological membranes are highly heterogeneous environments that support a wide array of biochemical and biophysical processes.[1−5] Lipids themselves are a diverse group of molecules with active roles in membrane-associated function through signaling,[5−8] lateral membrane organization,[4,9,10] and modulation of integral membrane protein function, including ion channels,[2,11−13] ATPases,[14−16] and G-protein-coupled receptors.[17] Despite biological significance, the role of lipids in the biophysics of heterogeneous membrane interfaces has not been fully characterized. The conjunction of lipid−lipid interactions and molecular crowding makes it challenging to study systems with diverse lipid populations.[3,18,19] Additionally, the lipid−water interface constitutes a hydrogen bond (H-bond) environment that is markedly different from that of bulk water, adding to the complexity of local dynamics.[20−22] Despite recent advances in modeling,[3,23−26] lipidomics,[27−30] imaging,[31] and spectroscopy,[21,32−36] mixed-lipid systems remain a challenge to characterize via both experiment and simulations.

The lipid−water interface is characterized by a network of H-bonds that stabilizes the lipid structure and drives dynamics of both water and lipid molecules.[37−40] Indeed, H-bond interactions are drastically different at hydrophobic−hydrophilic interfaces when compared to those at the bulk, as a result of confinement and interfacial H-bond donor/acceptor balance.[20,21,38,41−43] Lipids also exhibit a diverse array of headgroup structures, which vary in size, polarity, charge, and H-bond-donating and -accepting capacities, which strongly impact interfacial structure and dynamics.[29,41,42,44]

Though membrane phospholipids are highly diverse, phosphatidylcholine (PC) and phosphatidylethanolamine (PE) lipid species are significantly more abundant than any other phospholipid in both eukaryotes and prokaryotes.[27,45,46] PC and PE also have nearly identical molecular structures but different H-bond formation abilities due to differences in nitrogen substitution (Figure 1). Specifically, PC lipids have a quaternary ammonium with three methyl groups attached,

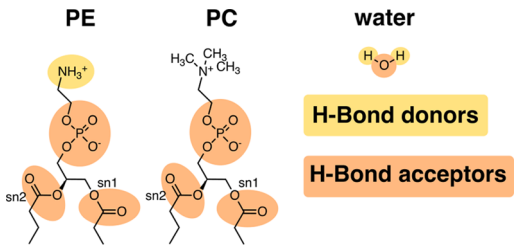

Figure 1. Functional groups present at the lipid−water interface in PC and PE lipids. Strong H-bond donors are shaded in mustard, and H-bond acceptors are shaded in orange. Unlike PC, PE lipids have polar protons that participate in H-bonding.

Received: September 25, 2020
Revised: December 11, 2020
Published: January 28, 2021

https://dx.doi.org/10.1021/acs.jpcb.0c08755
J. Phys. Chem. B 2021, 125, 1343−1350

while PE lipids have a primary ammonium, and as a result, PE lipids can both donate and accept H-bonds.[46] The difference in nitrogen substitution leads to differences in lipid membrane phase behavior,[47,48] curvature,[49] ion binding,[50] and structure.[51]

The distribution of PC and PE is highly heterogeneous across different membranes; in mammalian cells, for example, PE is highly enriched on the cytoplasmic leaflet of the plasma membrane, while high concentrations of PC lipids are present in both leaflets.[29] Traditionally, the different packing and organization of PC and PE lipids result from a balance of three closely related effects: (1) PE has less steric bulk in the headgroup region than PC, and as a result, PE lipids are described as having an intrinsic curvature;[46] (2) lacking the three methyl groups, PE lipids have less overall bulk than PC lipids, and as a result, packing density is increased;[52] and (3) direct lipid−lipid H-bonding in PE[52] further decreases the area-per-lipid. The importance of these factors is supported by a variety of findings, including measurements of area-per-lipid,[53,54] phase transition temperatures,[55,56] and characterization of lipid packing geometries.[49,51,57] Despite their presence across biological membranes and inherent structural effects, PE lipids have been largely understudied relative to PC lipids[46,47] due to their difficulty forming unsaturated planar membrane structures, which are used in numerous biophysical techniques including sum-frequency generation spectroscopy,[21] neutron and X-ray reflectometry,[58] NMR spectroscopy,[59,60] electrochemical sensors,[61] and fluorescence microscopy.[62] While planar membranes with up to 90 mol % PE can be prepared, PE concentrations above 50 mol % can lead to the formation of defects, which limit the reproducibility of experiments.[46]

In the present study, we use Fourier-transform infrared (FTIR) and ultrafast two-dimensional infrared (2D IR) spectroscopy of ester carbonyl vibrations (Figure 1) to characterize H-bond structure and dynamics at the hydrophobic−hydrophilic interface of mixed PC/PE membranes. Spectroscopic measurements are interpreted through molecular dynamics simulations with alchemical steps (MDAS)[26] to provide an atomistic perspective while ensuring full equilibration of the mixtures.

MATERIALS AND METHODS

Infrared Absorption Spectroscopy. Dipalmitoylphosphatidylethanolamine (DPPE) and dipalmitoylphosphatidylcholine (DPPC) were purchased from Avanti Polar Lipids and used without further purification. DPPE was dissolved in 65:25:4 $CHCl_3$/MeOH/H_2O, and DPPC was dissolved in $CHCl_3$ at 25 mg/mL. Samples of 1:1 DPPC/DPPE, 3:1 DPPC/DPPE, and 100% DPPC were prepared by combining lipid solutions in appropriate molar ratios and then evaporating the solvent under a dry nitrogen stream followed by vacuum desiccation. Lipid films were reconstituted in 0.15 M NaCl in D_2O at a concentration of 50 mg/mL. Samples were subjected to six freeze−thaw cycles and 20 min sonication at 60 °C prior to collecting FTIR measurements.

FTIR spectra were recorded on a Bruker Vertex 70 spectrometer. An aqueous suspension of 50 μL was held between two CaF2 windows separated by a 25 μm Teflon spacer. Samples were heated to 60 °C and equilibrated for 10 min using a brass sample cell and a recirculating chiller to ensure all lipid membranes were in the fluid phase. Before and during data collection, the spectrometer was purged with dry air to minimize perturbations from water vapor. Four samples were made for each lipid system, and infrared absorption spectra were independently collected for each sample.

Ultrafast 2D IR Spectroscopy. Mechanically aligned lipid multilayers[63−65] were used in 2D IR and pump−probe experiments. Lipid solutions, in the cosolvent system described above, were combined in appropriate molar ratios, and then an aliquot (1.5 mm total lipid) was drop-cast onto a CaF_2 window. The solvent was allowed to evaporate for several minutes at an ambient pressure and then further evaporated for an hour under a mild vacuum. A solution of 0.15 M NaCl in D_2O was pipetted onto the dried lipid film in a 1:1 D_2O/lipid mass ratio, another clean CaF_2 window was placed directly on top of the film, and the two windows were equilibrated at 60 °C and 100% relative humidity for an hour using a custom-built hydration chamber and a heated water bath. Following equilibration, the two windows were rotated relative to each other in the sample cell at 60 °C until proper optical quality (low scatter and a carbonyl optical density of approximately 0.5) was achieved. Before and after acquisition of 2D IR spectra, full hydration of the samples was checked by measuring FTIR spectra of the samples.

The 2D IR spectrometer has been described previously.[66] In brief, 100 fs mid-IR pulses were generated using an optical parametric amplifier and a difference frequency generation setup pumped by a Ti/sapphire laser (Astrella, Coherent Inc.). The mid-IR excitation pulses were generated by a pulse shaper (QuickShape, PhaseTech). The pump−probe delay was controlled by a delay stage. The 2D IR signal was measured using a spectrometer with a 128 × 128 pixel MCT array detector (Teledyne), which was also used to resolve the probe frequency axis. The pump frequency axis was resolved through a numerical Fourier transformation of the pump delay time. The pump and probe pulses were maintained at perpendicular polarizations to reduce pump scatter.

Molecular Dynamics Simulations. Three DPPC/DPPE bilayer mixtures with PC/PE ratios of 1:0 (pure DPPC), 3:1, and 1:1 were constructed using the CHARMM-GUI[67] interface with lipids distributed randomly across each 100-phospholipid leaflet. The bilayers were solvated with TIP3P water molecules and 0.15 M sodium chloride (NaCl). Each system consisted of approximately 50,000 atoms. Simulations were run using the CHARMM36 force field,[68] as implemented in the NAMD package of programs.[69] Each system was energy-minimized, then equilibrated in the NPT ensemble using the Langevin thermostat and Nose−Hoover barostat[70,71] at 333 K and 1 atm for 20 ns. The systems were then equilibrated in the NVT ensemble at 333 K for 10 ns. Waters were kept rigid using the SETTLE algorithm,[72] and all other bond lengths with hydrogen atoms were kept fixed with the SHAKE algorithm.[73] The time step used was 1 fs in all of the simulations. A real space cutoff distance of 12 Å was used, and particle mesh Ewald (PME)[74] was accounted for long-range electrostatic calculations. The 1:1 DPPC/DPPE system was selected to be equilibrated with the MDAS algorithm (Section S2) to explore further the equilibrium distribution and miscibility of the binary system. Upon confirming uniform mixing at the corresponding temperature, the production runs for each system were performed for 200 ns at the NVT ensemble. We note that the equilibration rate within the MDAS algorithm is about a factor of 1,000 faster than traditional MD simulations.[26]

Following MDAS equilibration, 100 ps trajectories were carried out to characterize the dynamics at the ester carbonyl

https://dx.doi.org/10.1021/acs.jpcb.0c08755
J. Phys. Chem. B 2021, 125, 1343−1350

position. Frames were saved every 20 fs to capture the fast fluctuations, and frequency shifts were calculated using an electrostatic map.[75]

RESULTS

Infrared Absorption Spectroscopy. The ester stretching mode is used as a probe of the interface, as the absorption frequency is sensitive to H-bonding to ester carbonyls, which are precisely positioned at the interface between hydrophobic and hydrophilic environments.[75] This sensitivity is well documented for lipids, which usually exhibit a 0 H-bond peak around 1745 cm^{-1} and a 1 H-bond peak around 1730 cm^{-1}.[76] Figure 2 shows IR absorption spectra of the ester

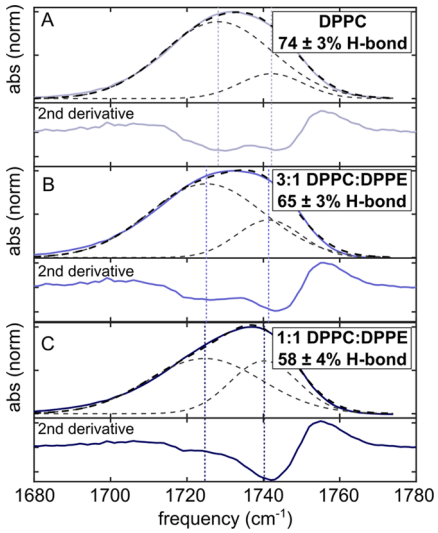

Figure 2. Absorption spectra of the ester carbonyl band of DPPC/DPPE lipid bilayers. Absorption (upper) and second-derivative (lower) spectra of the lipid ester band for (A) pure DPPC, (B) 3:1 DPPC/DPPE, and (C) 1:1 DPPC/DPPE lipid systems. Gaussian fits are shown by dashed lines, and the center frequencies of the Gaussian peaks are indicated by the dotted vertical bars. The insets show the populations along with the error bounds extracted from multiple replicates (see Figure S1).

carbonyls for DPPC and DPPC/DPPE mixed bilayers. Headgroup composition effects on H- bonding populations are quantified by fitting absorption spectra to a pair of Gaussian peaks centered within 2.0 cm^{-1} of the minima identified in the second-derivative plot. Indeed, the local minima in the second-derivative plots (Figure 2) agree with previous assignments.[76] The populations of each H-bond ensemble can then be extracted by integrating the area under each fit peak, as the relative peak areas are proportional to the number of lipid ester carbonyls with 0 or 1 H-bonds.[75,76] Repeated FTIR experiments were performed to determine the error in H-bond ensemble estimates (Figure S1), and temperature-dependent FTIR spectra were used to evaluate the relative oscillator strengths of the 0 H-bond and 1 H-bond peak (Section S1).

The C=O H-bond populations, shown in Figure 2, indicate that H-bonding decreases with increasing PE composition: in pure DPPC, 74% of the lipid carbonyls form H-bonds, while in the 1:1 DPPC/DPPE this value decreases to 58%, and an intermediate number of H-bonds to carbonyls are observed in 3:1 DPPC/DPPE. Similar to the shifts in peak frequency previously discussed, these H-bonding effects may in part be explained by the differences in lipid packing: PE increases the packing efficiency and decreases H-bond populations.

Molecular Dynamics Simulations. Atomistic MD trajectories provide a molecular interpretation of the measured IR absorption line shapes. The miscibility of DPPC and DPPE was tested using the MDAS enhanced sampling algorithm,[26,77] and phase separation was not observed. Further details are included in Section S2.

H-bond populations (Table 1) are extracted from the trajectories using geometric criteria:[78,79] < 0.35 nm donor (D)

Table 1. Average Number of H-Bonds to Lipid Ester Carbonyls Computed from MD Trajectories Using Geometric Criteria[a]

ester location	1:0 DPPC/DPPE	DPPC/DPPE 3:1	DPPC/DPPE 1:1
PC (sn-2)	0.52	0.51	0.50
PC (sn-1)	0.49	0.48	0.47
PE (sn-2)	N/A	0.49	0.49
PE (sn-1)	N/A	0.44	0.44
average	0.51	0.49	0.48

[a]See the text for details.

and acceptor (A) distance and a donor-hydrogen−acceptor angle of < 30°. Simulations show that the presence of DPPE led to decreased H-bonding to the ester carbonyls of DPPC. DPPE carbonyls experienced fewer H-bonds overall than DPPC carbonyls; however, the presence of DPPE resulted in decreased H-bonds to DPPC ester carbonyls. While simulations are in qualitative agreement with experiment, the magnitude of the effect is smaller in simulations, and the prevalence of H-bonds in experiment is higher than in simulations. For example, in experiment, 74% of the DPPC ester carbonyls experienced H-bonds versus approximately 50% in simulations. Additionally, the area-per-lipid was significantly decreased in the systems containing DPPE when compared to that of the pure DPPC system (Table S1).

In summary, simulations indicate that (1) DPPE decreases H-bonding to DPPC ester carbonyls at the lipid−water interface, (2) DPPE ester carbonyls form fewer H-bonds on average than DPPC ester carbonyls, and (3) DPPC and DPPE are well mixed on a molecular length scale.

Ultrafast 2D IR Spectroscopy. Complete characterization of the hydrophilic−hydrophobic interface includes probing the effects of the lipid headgroups on interfacial dynamics. Here, we expand upon the IR absorption results by using ultrafast 2D IR to measure the dynamics around the carbonyl probes. In brief, 2D IR spectra provide a correlation between a set of excitation (pump) frequencies and a set of detection (probe) frequencies. The changing environment around the oscillator results in loss of correlation between the pump and probe frequencies as the delay between the excitation and detection is increased. Specifically, 2D IR spectra of the lipid ester stretching vibration provide an autocorrelation of the carbonyl frequency fluctuations, referred to as the frequency−frequency correlation function (FFCF). Figure 3B shows four representative spectra of DPPC collected at different pump−probe delay times. The loss of correlation is observed as a horizontal rotation of the peak at longer delays. The full set of 2D IR spectra is included in Section S4. Multiple methods exist for extracting the FFCF from 2D IR peaks to describe dynamics.[80,81] The presence of partially overlapping peaks within the ester band necessitates peak fitting using the Kubo

https://dx.doi.org/10.1021/acs.jpcb.0c08755
J. Phys. Chem. B 2021, 125, 1343−1350

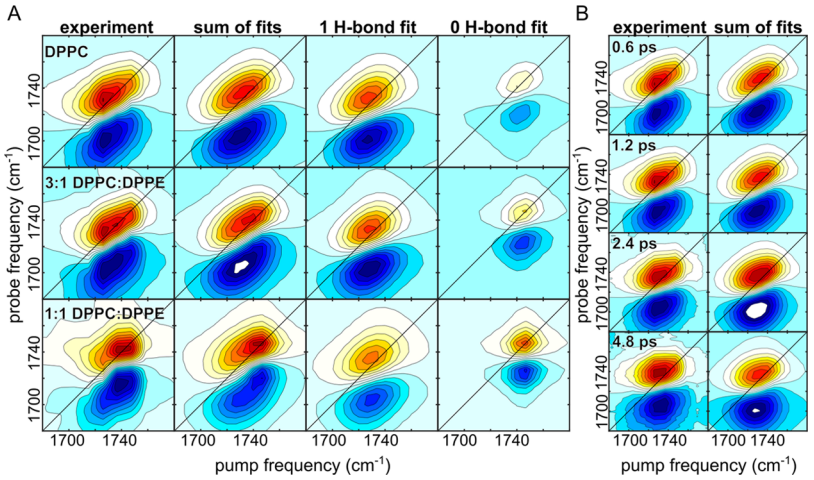

Figure 3. Experimental spectra of the ester carbonyl band of DPPC, 3:1 DPPC/DPPE, and 1:1 DPPC/DPPE. (A) 2D IR spectra of DPPC, 3:1 DPPC/DPPE, and 1:1 DPPC/DPPE (left) with Kubo line shape fits to the 0 and 1 H-bond peaks, and the total fit to the data. All spectra in panel A are plotted with a pump−probe delay time of 0.6 ps. (B) Waiting-time dependence of the experimental DPPC spectra and line shape fit.

line shape model.[82,83] Fitting the time-dependent 2D IR spectra at 34 separate time delays yields a set of two time-dependent peaks (Figure 3A), and the changes in each peak's shape are modeled by an FFCF. Within this model, the FFCF, $C(t)$, during the time scale of experiment is assumed to be an exponential decay of the form

$$C(t) = \Delta\omega^2 e^{-|t|/\tau_c} \quad (1)$$

in which $\Delta\omega$ is the amplitude of frequency fluctuations, τ_c is the correlation lifetime, and t is the time delay. A more detailed description of the fitting process is provided in Sections S3 and S4 with all spectra and fits (Figures S9−S14). Separate correlation times are assumed for the 1 H-bond and 0 H-bond peaks. The values of $\Delta\omega$ and τ_c obtained from fitting are tabulated in Table 2. In each system, the fluctuation magnitude, $\Delta\omega$, is greater in the 1 H-bond ester peak than in the 0 H-bond ester peak. We also observed a difference in dynamics; the 1 H-bond peak exhibited dynamics that were consistently faster than the 0 H-bond peak regardless of the PE content. The presence of PE had a pronounced effect on the time scale of the FFCF extracted using the Kubo model. The 1:1 DPPC/DPPE system exhibited the shortest correlation lifetimes, indicating fast dynamics, while the 3:1 DPPC/DPPE system exhibited slower dynamics, and the slowest dynamics were observed for pure DPPC. We were able to model the line shapes observed via 2D IR without accounting for chemical exchange, suggesting that the dynamics probed primarily describe fluctuating electric field amplitudes.[64]

Table 2. FFCF Parameters from Fitting to 2D IR Spectra

	1 H-bond		0 H-bond	
system	$\Delta\omega_{1Hb}$ (cm^{-1})	τ_{1Hb} (ps)	$\Delta\omega_{0Hb}$ (cm^{-1})	τ_{0HB} (ps)
1:0 DPPC/DPPE	13.4 ± 0.2	1.9 ± 0.1	6.6 ± 0.2	9 ± 1
3:1 DPPC/DPPE	12.4 ± 0.2	1.7 ± 0.1	5.7 ± 0.1	4 ± 1
1:1 DPPC/DPPE	13.4 ± 0.4	1.4 ± 0.2	4.1 ± 0.2	2.3 ± 0.5

Electrostatic autocorrelations were also calculated from the MD trajectories of the lipid membranes as a point of comparison between experiment and simulations (Table S4 and Figure S15). These autocorrelations were fit to a function of the form

$$C(t) = a_1 e^{-t/\tau_{c1}} + a_2 e^{-t/\tau_{c2}} + a_3 e^{-t/\tau_{c3}} \quad (2)$$

where the parameters a_1, a_2, and a_3 describe the amplitudes and τ_{c1}, τ_{c2}, and τ_{c3} describe the decay constants of the three exponentials, respectively. The three decay constants appear in the range of ∼20−40, ∼250, and 3−4 ps, respectively. The slowest component is compared directly with the experimental value of the FFCF. The fastest dynamics were observed in the 3:1 DPPC/DPPE system, with correlation times of 3.5 ps, while the correlation times for the 1:1 DPPC/DPPE system and pure DPPC system each were fit to correlation times between 3.8 and 4.0 ps. Correlation times were slightly faster for DPPE than for DPPC. Trends in FFCF lifetimes from simulations were not identical to trends obtained from experiment; however, they allow for a direct comparison between experiment and simulation.

DISCUSSION

Two dynamic processes are measurable via 2D IR spectroscopy of the ester carbonyl stretches: (1) local electric field fluctuations observed through the FFCF of individual peaks and (2) H-bond breaking and formation observed through cross-peak growth. Within our PC/PE system, electric field fluctuations were faster for DPPC/DPPE mixtures than for pure DPPC membrane.

Local Electrostatic Fluctuations. Fluctuation dynamics, quantified through the FFCF, were faster in densely packed membranes with high DPPE concentrations and a relatively low proportion of H-bond ester carbonyls. This measured trend mirrors the effect observed in surfactant interfaces; increased packing density is associated with decreased H-bonding to water accompanied by faster FFCF dynamics.[84] Water at interfaces exhibits slow dynamics due to constraints to the H-bond network. Interfacial water molecules have fewer possible H-bond configurations than bulk water molecules and are thus increasingly constrained. The presence of constrained interfacial water in the membrane slows the conformational fluctuations in the lipid headgroup region, and therefore measured differences in dynamics between the 1:1 DPPC/DPPE, 3:1 DPPC/DPPE, and DPPC systems can be

https://dx.doi.org/10.1021/acs.jpcb.0c08755
J. Phys. Chem. B 2021, 125, 1343−1350

rationalized in terms of differing levels of interfacial hydration resulting from changes in the packing density.

Measured 2D IR dynamics also differed between the 1 H-bond and 0 H-bond peaks. Electric field fluctuations had a greater magnitude in the 1 H-bond peak than in the 0 H-bond peak, as evidenced by the difference in inhomogeneous line widths, which may be explained in part by the large fields produced by the partial charges of primary amines and water molecules. In addition, ester carbonyls contributing to the 1 H-bond peak experience stronger static electric fields than those contributing to the 0 H-bond peak, which is evidenced by the 15 cm^{-1} red shift of the 1 H-bond peak relative to the 0 H-bond peak. Differences in the time scales of the fluctuations were also observed between the two component peaks: dynamics were faster for the 1 H-bond peak than for the 0 H-bond peak across all three systems. Relatively slow fluctuations for the 0 H-bond carbonyls have been observed previously; however, the source of the slowdown remains unclear.[64] At first glance, the two results from the FFCF may appear contradictory; the interfacial dynamics are fastest in the system with the fewest H-bonds to the ester carbonyls, but the 1 H-bond peak exhibits faster dynamics than the 0 H-bond peak. One possible explanation may lie in the role of molecular orientation, and not just proximity, in H-bond formation. Interfacial water is vibrationally coupled to the esters in both the 1 H-bond and 0 H-bond peaks,[85] indicating that the carbonyls in the 0 H-bond and 1 H-bond peaks are both similarly exposed to interfacial water. The differences between the 0 H-bond peak and 1 H-bond peak may then be more closely related to the orientations of esters than their proximity to water since H-bonds require both proximity and the proper orientation to exist. Indeed, there are significant differences in the orientations of esters in these peaks.[86] H-bonded ester carbonyl dipoles are oriented, on average, toward the lipid−water interface, while 0 H-bond dipoles are oriented away from the lipid−water interface. Thus, the trends observed between the 0 H-bond and 1 H-bond peaks do not contradict the composition-dependent trends observed between DPPC, 3:1 DPPC/DPPE, and 1:1 DPPC/DPPE.

Trends in electrostatic fluctuations were not reproduced quantitatively in simulations. In the 2D IR spectra, the slowest electrostatic fluctuations were observed in the DPPC membrane and the fastest fluctuations were observed in the 1:1 DPPC/DPPE membrane, while in simulations the fluctuations were fastest in the 3:1 DPPC/DPPE membrane. There are multiple factors that may play a role in this difference: (1) the 1 H-bond and 0 H-bond peaks arise from esters with distinct orientational distributions.[86] The difference in orientation between 1 H-bond and 0 H-bond ester carbonyls is not captured by simulations, which can limit comparison between simulations and experiments that probe the lipid esters. (2) The trajectories utilized TIP3P water, which may produce faster dynamics compared to experiment,[87] although TIP3P has been used previously to reproduce experimental trends in lipid dynamics.[88,89]

Interfacial H-Bond Interactions. In our 2D IR experiments, the H-bond rates were too slow to be measured precisely, as the carbonyl vibrational lifetime (~1.5 ps) limits the acquisition of 2D IR spectra to several picoseconds. However, the FTIR spectroscopy utilized here provides insight into the H-bond equilibrium at the hydrophilic−hydrophobic interface of the lipid bilayer. The esters used as vibrational probes are adjacent to both the headgroups and tails of the lipids and, as such, probe the interface between the hydrophilic and hydrophobic regions of the lipid membrane.

Recent ultrafast studies have shown that lipids with H-bond-donating primary amine headgroups slow down dynamics at the lipid−water interface much more than lipids with tertiary amine headgroups, which cannot donate H-bonds.[90] Here, we found a separate set of changes to ultrafast dynamics at the interface between the hydrophilic headgroup region of the membrane and the hydrophobic bilayer core, rather than the interface between water and the lipid headgroups. The effects of PE headgroups on the dynamics at the hydrophilic−hydrophobic interface are striking, given that the structural differences between PC/PE lipids are exclusive to the ammonium group at the boundary between the headgroup region and water, while the functional groups probed here occupy a completely different region of the membrane. These depth-dependent changes in dynamics have implications for the function and structure of integral membrane proteins, which exist in membranes with high concentrations of both PC and PE lipids. Specific examples of membrane proteins with preferential interactions involving PE lipids are already abundant,[14,91,92] and as integral membrane proteins cross through the entire lipid membrane, the differential effects of PC and PE at the hydrophilic/hydrophobic interface are likely to be crucial for understanding lipid−protein interactions.

CONCLUSIONS

Phosphatidylethanolamine (PE) and phosphatidylcholine (PC) headgroups are the most common phospholipid headgroups in eukaryotes; however, PC−PE interactions still remain largely unexplored on a molecular time and length scale. Through a combination of linear infrared spectroscopy, ultrafast 2D IR spectroscopy, and molecular dynamics simulations, we have characterized the effects of PC and PE headgroups on dynamics and intermolecular interactions in lipid membranes. Within the interface between polar and nonpolar regions of lipid membranes, the presence of H-bond-donating headgroups leads to an increase in dynamics on a sub-ns time scale. Additionally, the number of C═O H-bonds in this region decreases with increasing PE content, as PE lipids pack together more closely than PC lipids. Taken together, these results suggest that interfacial water drives dynamics at the lipid−water interface and that lipid−lipid H-bonds are implicated in complex depth-dependent interfacial dynamics. These results have implications for membrane protein folding, bilayer organization, and lipid−peptide interactions. Further work will be required to bring these results to the full context of heterogeneous multicomponent biological membranes, which contain high concentrations of both PC and PE lipids.

ASSOCIATED CONTENT

Supporting Information

The Supporting Information is available free of charge at https://pubs.acs.org/doi/10.1021/acs.jpcb.0c08755.

Computational methods, molecular dynamics results, and ultrafast 2D IR spectra (PDF)

AUTHOR INFORMATION

Corresponding Author

Carlos R. Baiz − *Department of Chemistry, University of Texas at Austin, Austin, Texas 78712-1224, United States;*

https://dx.doi.org/10.1021/acs.jpcb.0c08755
J. Phys. Chem. B 2021, 125, 1343−1350

orcid.org/0000-0003-0699-8468; Email: cbaiz@cm.utexas.edu

Authors

Mason L. Valentine − *Department of Chemistry, University of Texas at Austin, Austin, Texas 78712-1224, United States*

Maya K. Waterland − *Department of Chemistry, University of Texas at Austin, Austin, Texas 78712-1224, United States*

Arman Fathizadeh − *Oden Institute for Computational Science and Engineering, Austin, Texas 78712, United States*

Ron Elber − *Department of Chemistry, University of Texas at Austin, Austin, Texas 78712-1224, United States; Oden Institute for Computational Science and Engineering, Austin, Texas 78712, United States;* orcid.org/0000-0001-7849-415X

Complete contact information is available at: https://pubs.acs.org/10.1021/acs.jpcb.0c08755

Author Contributions

All authors contributed to the design and conduction of the work. All authors contributed to editing the manuscript. Manuscript text and figures were prepared by M.L.V., A.F., and M.K.W. Simulations and MDAS method development were performed by A.F. Infrared spectroscopy was performed by M.L.V. and M.K.W.

Notes

The authors declare no competing financial interest.

■ ACKNOWLEDGMENTS

C.R.B. and R.E. acknowledge funding from the Welch Foundation (F-1891 and F-1896, respectively) and acknowledge support from the National Science Foundation (BIO-1815354). R.E. acknowledges grant NIH GM111364 for support.

■ REFERENCES

(1) Corradi, V.; Sejdiu, B. I.; Mesa-Galloso, H.; Abdizadeh, H.; Noskov, S. Yu.; Marrink, S. J.; Tieleman, D. P. Emerging Diversity in Lipid−Protein Interactions. *Chem. Rev.* **2019**, *119*, 5775−5848.

(2) Poveda, J. A.; Giudici, A. M.; Renart, M. L.; Millet, O.; Morales, A.; González-Ros, J. M.; Oakes, V.; Furini, S.; Domene, C. Modulation of the Potassium Channel KcsA by Anionic Phospholipids: Role of Arginines at the Non-Annular Lipid Binding Sites. *Biochim. Biophys. Acta, Biomembr.* **2019**, No. 183029.

(3) Marrink, S. J.; Corradi, V.; Souza, P. C. T.; Ingólfsson, H. I.; Tieleman, D. P.; Sansom, M. S. P. Computational Modeling of Realistic Cell Membranes. *Chem. Rev.* **2019**, *119*, No. 6184.

(4) Engelman, D. M. Membranes Are More Mosaic than Fluid. *Nature* **2005**, *438*, 578−580.

(5) Lizardo, D. Y.; Parisi, L. R.; Li, N.; Atilla-Gokcumen, G. E. Noncanonical Roles of Lipids in Different Cellular Fates. *Biochemistry* **2017**, *57*, 22−29.

(6) Zhang, Z.; Jiang, X.; Xu, D.; Zheng, W.; Liu, M.; Li, C. Calcium Accelerates SNARE-Mediated Lipid Mixing through Modulating α-Synuclein Membrane Interaction. *Biochim. Biophys. Acta, Biomembr.* **2018**, *1860*, 1848−1853.

(7) Wong, R.; Hadjiyanni, I.; Wei, H.-C.; Polevoy, G.; McBride, R.; Sem, K.-P.; Brill, J. A. PIP2 Hydrolysis and Calcium Release Are Required for Cytokinesis in Drosophila Spermatocytes. *Curr. Biol.* **2005**, *15*, 1401−1406.

(8) Leventis, P. A.; Grinstein, S. The Distribution and Function of Phosphatidylserine in Cellular Membranes. *Annu. Rev. Biophys.* **2010**, *39*, 407−427.

(9) Wen, Y.; Vogt, V. M.; Feigenson, G. W. Multivalent Cation-Bridged PI(4,5)P 2 Clusters Form at Very Low Concentrations. *Biophys. J.* **2018**, *114*, 2630−2639.

(10) Cebecauer, M.; Amaro, M.; Jurkiewicz, P.; Sarmento, M. J.; Šachl, R.; Cwiklik, L.; Hof, M. Membrane Lipid Nanodomains. *Chem. Rev.* **2018**, *118*, 11259−11297.

(11) Hénault, C. M.; Govaerts, C.; Spurny, R.; Brams, M.; Estrada-Mondragon, A.; Lynch, J.; Bertrand, D.; Pardon, E.; Evans, G. L.; Woods, K.; et al. A Lipid Site Shapes the Agonist Response of a Pentameric Ligand-Gated Ion Channel. *Nat. Chem. Biol.* **2019**, 1−9.

(12) Kumar, P.; Wang, Y.; Zhang, Z.; Zhao, Z.; Cymes, G. D.; Tajkhorshid, E.; Grosman, C. Cryo-EM Structures of a Lipid-Sensitive Pentameric Ligand-Gated Ion Channel Embedded in a Phosphatidylcholine-Only Bilayer. *Proc. Natl. Acad. Sci. U.S.A.* **2020**, *117*, No. 1788.

(13) Phillips, R.; Ursell, T.; Wiggins, P.; Sens, P. Emerging Roles for Lipids in Shaping Membrane-Protein Function. *Nature* **2009**, *459*, 379−385.

(14) Gantzel, R. H.; Mogensen, L. S.; Mikkelsen, S. A.; Vilsen, B.; Molday, R. S.; Vestergaard, A. L.; Andersen, J. P. Disease Mutations Reveal Residues Critical to the Interaction of P4-ATPases with Lipid Substrates. *Sci. Rep.* **2017**, *7*, No. 628.

(15) Hidalgo, C.; Thomas, D. D.; Ikemoto, N. Effect of the Lipid Environment on Protein Motion and Enzymatic Activity of Sarcoplasmic Reticulum Calcium ATPase. *J. Biol. Chem.* **1978**, *253*, 6879−6887.

(16) Hunter, G. W.; Negash, S.; Squier, T. C. Phosphatidylethanolamine Modulates Ca-ATPase Function and Dynamics. *Biochemistry* **1999**, *38*, 1356−1364.

(17) Niu, S.-L.; Mitchell, D. C.; Litman, B. J. Optimization of Receptor-G Protein Coupling by Bilayer Lipid Composition II: Formation of Metarhodopsin II-Transducin Complex. *J. Biol. Chem.* **2001**, *276*, 42807−42811.

(18) Melcrová, A.; Pokorna, S.; Vosahlikova, M.; Sykora, J.; Svoboda, P.; Hof, M.; Cwiklik, L.; Jurkiewicz, P. Concurrent Compression of Phospholipid Membranes by Calcium and Cholesterol. *Langmuir* **2019**, No. 11358.

(19) Hirai, M.; Ajito, S.; Arai, S.; Adachi, M.; Shimizu, R.; Wakamatsu, K.; Takata, S.; Iwase, H. Observation of Protein and Lipid Membrane Structures in a Model Mimicking the Molecular Crowding Environment of Cells Using Neutron Scattering and Cell Debris. *J. Phys. Chem. B* **2019**, *123*, No. 3189.

(20) Singh, P. C.; Inoue, K.; Nihonyanagi, S.; Yamaguchi, S.; Tahara, T. Femtosecond Hydrogen Bond Dynamics of Bulk-like and Bound Water at Positively and Negatively Charged Lipid Interfaces Revealed by 2D HD-VSFG Spectroscopy. *Angew. Chem., Int. Ed.* **2016**, *55*, 10621−10625.

(21) Inoue, K.; Singh, P. C.; Nihonyanagi, S.; Yamaguchi, S.; Tahara, T. Cooperative Hydrogen-Bond Dynamics at a Zwitterionic Lipid/Water Interface Revealed by 2D HD-VSFG Spectroscopy. *J. Phys. Chem. Lett.* **2017**, *8*, 5160−5165.

(22) Lee, E.; Kundu, A.; Jeon, J.; Cho, M. Water Hydrogen-Bonding Structure and Dynamics near Lipid Multibilayer Surface: Molecular Dynamics Simulation Study with Direct Experimental Comparison. *J. Chem. Phys.* **2019**, *151*, No. 114705.

(23) Wu, E. L.; Cheng, X.; Jo, S.; Rui, H.; Song, K. C.; Dávila-Contreras, E. M.; Qi, Y.; Lee, J.; Monje-Galvan, V.; Venable, R. M.; et al. CHARMM-GUI Membrane Builder toward Realistic Biological Membrane Simulations. *J. Comput. Chem.* **2014**, *35*, 1997−2004.

(24) Gu, R.-X.; Baoukina, S.; Tieleman, D. P. Phase Separation in Atomistic Simulations of Model Membranes. *J. Am. Chem. Soc.* **2020**, *142*, No. 2844.

(25) Ingólfsson, H. I.; Melo, M. N.; van Eerden, F. J.; Arnarez, C.; Lopez, C. A.; Wassenaar, T. A.; Periole, X.; de Vries, A. H.; Tieleman, D. P.; Marrink, S. J. Lipid Organization of the Plasma Membrane. *J. Am. Chem. Soc.* **2014**, *136*, 14554−14559.

(26) Fathizadeh, A.; Elber, R. A Mixed Alchemical and Equilibrium Dynamics to Simulate Heterogeneous Dense Fluids: Illustrations for

Lennard-Jones Mixtures and Phospholipid Membranes. *J. Chem. Phys.* **2018**, *149*, No. 072325.
(27) Klose, C.; Surma, M. A.; Simons, K. Organellar Lipidomics—Background and Perspectives. *Curr. Opin. Cell Biol.* **2013**, *25*, 406−413.
(28) Cajka, T.; Fiehn, O. Toward Merging Untargeted and Targeted Methods in Mass Spectrometry-Based Metabolomics and Lipidomics. *Anal. Chem.* **2016**, *88*, 524−545.
(29) Lorent, J. H.; Levental, K. R.; Ganesan, L.; Rivera-Longsworth, G.; Sezgin, E.; Doktorova, M.; Lyman, E.; Levental, I. Plasma Membranes Are Asymmetric in Lipid Unsaturation, Packing and Protein Shape. *Nat. Chem. Biol.* **2020**, *16*, 644−652.
(30) Bogdanov, M.; Pyrshev, K.; Yesylevskyy, S.; Ryabichko, S.; Boiko, V.; Ivanchenko, P.; Kiyamova, R.; Guan, Z.; Ramseyer, C.; Dowhan, W. Phospholipid Distribution in the Cytoplasmic Membrane of Gram-Negative Bacteria Is Highly Asymmetric, Dynamic, and Cell Shape-Dependent. *Sci. Adv.* **2020**, *6*, No. eaaz6333.
(31) Gramse, G.; Dols-Perez, A.; Edwards, M. A.; Fumagalli, L.; Gomila, G. Nanoscale Measurement of the Dielectric Constant of Supported Lipid Bilayers in Aqueous Solutions with Electrostatic Force Microscopy. *Biophys. J.* **2013**, *104*, 1257−1262.
(32) Block, S.; Aćimović, S. S.; Odebo Länk, N.; Käll, M.; Höök, F. Antenna-Enhanced Fluorescence Correlation Spectroscopy Resolves Calcium-Mediated Lipid−Lipid Interactions. *ACS Nano* **2018**, *12*, 3272−3279.
(33) Heberle, F. A.; Buboltz, J. T.; Stringer, D.; Feigenson, G. W. Fluorescence Methods to Detect Phase Boundaries in Lipid Bilayer Mixtures. *Biochim. Biophys. Acta, Mol. Cell Res.* **2005**, *1746*, 186−192.
(34) De Angelis, A. A.; Opella, S. J. Bicelle Samples for Solid-State NMR of Membrane Proteins. *Nat. Protoc.* **2007**, *2*, 2332−2338.
(35) Schmidt, M. L.; Davis, J. H. 2 H NMR of Oriented Phospholipid/Cholesterol Bilayers Containing an Amphiphilic Peptide. *Biochim. Biophys. Acta, Biomembr.* **2020**, *1862*, No. 183196.
(36) Jones, A. C.; Kearns, N. M.; Bohlmann Kunz, M.; Flach, J. T.; Zanni, M. T. Multidimensional Spectroscopy on the Microscale: Development of a Multimodal Imaging System Incorporating 2D White-Light Spectroscopy, Broadband Transient Absorption, and Atomic Force Microscopy. *J. Phys. Chem. A* **2019**, *123*, No. 10824.
(37) Karathanou, K.; Bondar, A.-N. Dynamic Water Hydrogen-Bond Networks at the Interface of a Lipid Membrane Containing Palmitoyl-Oleoyl Phosphatidylglycerol. *J. Membr. Biol.* **2018**, 1−13.
(38) Kundu, A.; Verma, P. K.; Ha, J.-H.; Cho, M. Studying Water Hydrogen-Bonding Network near the Lipid Multibilayer with Multiple IR Probes. *J. Phys. Chem. A* **2017**, *121*, 1435−1441.
(39) Inoue, K.; Nihonyanagi, S.; Tahara, T. Ultrafast Vibrational Dynamics at Aqueous Interfaces Studied by 2D Heterodyne-Detected Vibrational Sum Frequency Generation Spectroscopy. In *Coherent Multidimensional Spectroscopy*; Cho, M., Ed.; Springer Series in Optical Sciences; Springer: Singapore, 2019; pp 215−236. https://doi.org/10.1007/978-981-13-9753-0_10.
(40) Mason, J. T.; O'Leary, T. J. Effects of Headgroup Methylation and Acyl Chain Length on the Volume of Melting of Phosphatidylethanolamines. *Biophys. J.* **1990**, *58*, 277−281.
(41) Bhide, S. Y.; Berkowitz, M. L. Structure and Dynamics of Water at the Interface with Phospholipid Bilayers. *J. Chem. Phys.* **2005**, *123*, No. 224702.
(42) Skinner, J. L.; Pieniazek, P. A.; Gruenbaum, S. M. Vibrational Spectroscopy of Water at Interfaces. *Acc. Chem. Res.* **2012**, *45*, 93−100.
(43) Deplazes, E.; Sarrami, F.; Poger, D. Effect of H3O+ on the Structure and Dynamics of Water at the Interface with Phospholipid Bilayers. *J. Phys. Chem. B* **2020**, *124*, 1361−1373.
(44) Pullanchery, S.; Yang, T.; Cremer, P. S. Introduction of Positive Charges into Zwitterionic Phospholipid Monolayers Disrupts Water Structure Whereas Negative Charges Enhances It. *J. Phys. Chem. B* **2018**, *122*, 12260−12270.
(45) Marsh, D. *Handbook of Lipid Bilayers*, 2nd ed.; CRC Press: Boca Raton, Florida, 2013.
(46) Sendecki, A. M.; Poyton, M. F.; Baxter, A. J.; Yang, T.; Cremer, P. S. Supported Lipid Bilayers with Phosphatidylethanolamine as the Major Component. *Langmuir* **2017**, *33*, 13423−13429.
(47) Lewis, R. N.; McElhaney, R. N. Calorimetric and Spectroscopic Studies of the Polymorphic Phase Behavior of a Homologous Series of N-Saturated 1,2-Diacyl Phosphatidylethanolamines. *Biophys. J.* **1993**, *64*, 1081−1096.
(48) Cheng, K. H. Infrared Study of the Polymorphic Phase Behavior of Dioleoylphosphatidylethanolamine and Dioleoylphosphatidylcholine Mixtures. *Chem. Phys. Lipids* **1991**, *60*, 119−125.
(49) Marsh, D. Intrinsic Curvature in Normal and Inverted Lipid Structures and in Membranes. *Biophys. J.* **1996**, *70*, 2248−2255.
(50) Poyton, M. F.; Sendecki, A. M.; Cong, X.; Cremer, P. S. Cu2+ Binds to Phosphatidylethanolamine and Increases Oxidation in Lipid Membranes. *J. Am. Chem. Soc.* **2016**, *138*, 1584−1590.
(51) McIntosh, T. J. Differences in Hydrocarbon Chain Tilt between Hydrated Phosphatidylethanolamine and Phosphatidylcholine Bilayers. A Molecular Packing Model. *Biophys. J.* **1980**, *29*, 237−245.
(52) Brown, M. F. Soft Matter in Lipid−Protein Interactions. *Annu. Rev. Biophys.* **2017**, *46*, 379−410.
(53) Thurmond, R. L.; Dodd, S. W.; Brown, M. F. Molecular Areas of Phospholipids as Determined by 2H NMR Spectroscopy. Comparison of Phosphatidylethanolamines and Phosphatidylcholines. *Biophys. J.* **1991**, *59*, 108−113.
(54) Bouchet, A. M.; Frías, M. A.; Lairion, F.; Martini, F.; Almaleck, H.; Gordillo, G.; Disalvo, E. A. Structural and Dynamical Surface Properties of Phosphatidylethanolamine Containing Membranes. *Biochim. Biophys. Acta, Biomembr.* **2009**, *1788*, 918−925.
(55) Shimshick, E. J.; McConnell, H. M. Lateral Phase Separation in Phospholipid Membranes. *Biochemistry* **1973**, *12*, 2351−2360.
(56) Blume, A. Thermotropic Behavior of Phosphatidylethanolamine-Cholesterol and Phosphatidylethanolamine-Phosphatidylcholine-Cholesterol Mixtures. *Biochemistry* **1980**, *19*, 4908−4913.
(57) Petrache, H. I.; Dodd, S. W.; Brown, M. F. Area per Lipid and Acyl Length Distributions in Fluid Phosphatidylcholines Determined by (2)H NMR Spectroscopy. *Biophys. J.* **2000**, *79*, 3172−3192.
(58) Sturm, M.; Gutowski, O.; Brezesinski, G. The Influence of Calcium Traces in Ultrapure Water on the Lateral Organization in Tetramyristoyl Cardiolipin Monolayers. *ChemPhysChem* **2019**, *20*, 1−7.
(59) Arnold, A.; Labrot, T.; Oda, R.; Dufourc, E. J. Cation Modulation of Bicelle Size and Magnetic Alignment as Revealed by Solid-State NMR and Electron Microscopy. *Biophys. J.* **2002**, *83*, 2667−2680.
(60) Ferreira, T. M.; Coreta-Gomes, F.; Ollila, O. H. S.; Moreno, M. J.; Vaz, W. L. C.; Topgaard, D. Cholesterol and POPC Segmental Order Parameters in Lipid Membranes: Solid State 1H−13C NMR and MD Simulation Studies. *Phys. Chem. Chem. Phys.* **2013**, *15*, 1976−1989.
(61) Kawan, M.; Hidalgo, T. C.; Du, W.; Pappa, A.-M.; Owens, R. M.; McCulloch, I.; Inal, S. Monitoring Supported Lipid Bilayers with N-Type Organic Electrochemical Transistors. *Mater. Horiz.* **2020**, *7*, No. 2348.
(62) Castellana, E. T.; Cremer, P. S. Solid Supported Lipid Bilayers: From Biophysical Studies to Sensor Design. *Surf. Sci. Rep.* **2006**, *61*, 429−444.
(63) Kel, O.; Tamimi, A.; Thielges, M. C.; Fayer, M. D. Ultrafast Structural Dynamics Inside Planar Phospholipid Multibilayer Model Cell Membranes Measured with 2D IR Spectroscopy. *J. Am. Chem. Soc.* **2013**, *135*, 11063−11074.
(64) Stevenson, P.; Tokmakoff, A. Ultrafast Fluctuations of High Amplitude Electric Fields in Lipid Membranes. *J. Am. Chem. Soc.* **2017**, *139*, 4743−4752.
(65) Relat-Goberna, J.; Beedle, A. E. M.; Garcia-Manyes, S. The Nanomechanics of Lipid Multibilayer Stacks Exhibits Complex Dynamics. *Small* **2017**, *13*, No. 1700147.
(66) Edington, S. C.; Gonzalez, A.; Middendorf, T. R.; Halling, D. B.; Aldrich, R. W.; Baiz, C. R. Coordination to Lanthanide Ions

Distorts Binding Site Conformation in Calmodulin. *Proc. Natl. Acad. Sci. U.S.A.* **2018**, *115*, E3126−E3134.
(67) Jo, S.; Lim, J. B.; Klauda, J. B.; Im, W. CHARMM-GUI Membrane Builder for Mixed Bilayers and Its Application to Yeast Membranes. *Biophys. J.* **2009**, *97*, 50−58.
(68) Klauda, J. B.; Venable, R. M.; Freites, J. A.; O'Connor, J. W.; Tobias, D. J.; Mondragon-Ramirez, C.; Vorobyov, I.; MacKerell, A. D.; Pastor, R. W. Update of the CHARMM All-Atom Additive Force Field for Lipids: Validation on Six Lipid Types. *J. Phys. Chem. B* **2010**, *114*, 7830−7843.
(69) Huang, J.; Rauscher, S.; Nawrocki, G.; Ran, T.; Feig, M.; de Groot, B. L.; Grubmüller, H.; MacKerell, A. D. CHARMM36m: An Improved Force Field for Folded and Intrinsically Disordered Proteins. *Nat. Methods* **2017**, *14*, 71−73.
(70) Feller, S. E.; Zhang, Y.; Pastor, R. W.; Brooks, B. R. Constant Pressure Molecular Dynamics Simulation: The Langevin Piston Method. *J. Chem. Phys.* **1995**, *103*, 4613−4621.
(71) Feller, S. E.; Venable, R. M.; Pastor, R. W. Computer Simulation of a DPPC Phospholipid Bilayer: Structural Changes as a Function of Molecular Surface Area. *Langmuir* **1997**, *13*, 6555−6561.
(72) Miyamoto, S.; Kollman, P. A. Settle: An Analytical Version of the SHAKE and RATTLE Algorithm for Rigid Water Models. *J. Comput. Chem.* **1992**, *13*, 952−962.
(73) Ryckaert, J.-P.; Ciccotti, G.; Berendsen, H. J. C. Numerical Integration of the Cartesian Equations of Motion of a System with Constraints: Molecular Dynamics of n-Alkanes. *J. Comput. Phys.* **1977**, *23*, 327−341.
(74) Essmann, U.; Perera, L.; Berkowitz, M. L.; Darden, T.; Lee, H.; Pedersen, L. G. A Smooth Particle Mesh Ewald Method. *J. Chem. Phys.* **1995**, *103*, 8577−8593.
(75) Edington, S. C.; Flanagan, J. C.; Baiz, C. R. An Empirical IR Frequency Map for Ester C═O Stretching Vibrations. *J. Phys. Chem. A* **2016**, *120*, 3888−3896.
(76) Hübner, W.; Blume, A. Interactions at the Lipid−Water Interface. *Chem. Phys. Lipids* **1998**, *96*, 99−123.
(77) Fathizadeh, A.; Valentine, M.; Baiz, C. R.; Elber, R. Phase Transition in a Heterogeneous Membrane: Atomically Detailed Picture. *J. Phys. Chem. Lett.* **2020**, *11*, 5263−5267.
(78) Abraham, M. J.; Murtola, T.; Schulz, R.; Páll, S.; Smith, J. C.; Hess, B.; Lindahl, E. GROMACS: High Performance Molecular Simulations through Multi-Level Parallelism from Laptops to Supercomputers. *SoftwareX* **2015**, *1−2*, 19−25.
(79) van der Spoel, D.; van Maaren, P. J.; Larsson, P.; Tîmneanu, N. Thermodynamics of Hydrogen Bonding in Hydrophilic and Hydrophobic Media. *J. Phys. Chem. B* **2006**, *110*, 4393−4398.
(80) Kwak, K.; Rosenfeld, D. E.; Fayer, M. D. Taking Apart the Two-Dimensional Infrared Vibrational Echo Spectra: More Information and Elimination of Distortions. *J. Chem. Phys.* **2008**, *128*, No. 204505.
(81) Guo, Q.; Pagano, P.; Li, Y.-L.; Kohen, A.; Cheatum, C. M. Line Shape Analysis of Two-Dimensional Infrared Spectra. *J. Chem. Phys.* **2015**, *142*, No. 212427.
(82) Hamm, P.; Zanni, M. T. *Concepts and Methods of 2D Infrared Spectroscopy*; Cambridge University Press: Cambridge, UK, 2011.
(83) Yuan, R.; Fayer, M. D. Dynamics of Water Molecules and Ions in Concentrated Lithium Chloride Solutions Probed with Ultrafast 2D IR Spectroscopy. *J. Phys. Chem. B* **2019**, *123*, 7628−7639.
(84) Baryiames, C. P.; Teel, M.; Baiz, C. R. Interfacial H-Bond Dynamics in Reverse Micelles: The Role of Surfactant Heterogeneity. *Langmuir* **2019**, *35*, 11463−11470.
(85) Volkov, V. V.; Nuti, F.; Takaoka, Y.; Chelli, R.; Papini, A. M.; Righini, R. Hydration and Hydrogen Bonding of Carbonyls in Dimyristoyl-Phosphatidylcholine Bilayer. *J. Am. Chem. Soc.* **2006**, *128*, 9466−9471.
(86) Dreier, L. B.; Bonn, M.; Backus, E. H. G. Hydration and Orientation of Carbonyl Groups in Oppositely Charged Lipid Monolayers on Water. *J. Phys. Chem. B* **2019**, *123*, 1085−1089.
(87) Mark, P.; Nilsson, L. Structure and Dynamics of the TIP3P, SPC, and SPC/E Water Models at 298 K. *J. Phys. Chem. A* **2001**, *105*, 9954−9960.
(88) Venkatraman, R. K.; Baiz, C. R. Ultrafast Dynamics at the Lipid−Water Interface: DMSO Modulates H-Bond Lifetimes. *Langmuir* **2020**, *36*, 6502−6511.
(89) Flanagan, J. C.; Cardenas, A. E.; Baiz, C. R. Ultrafast Spectroscopy of Lipid−Water Interfaces: Transmembrane Crowding Drives H-Bond Dynamics. *J. Phys. Chem. Lett.* **2020**, *11*, 4093−4098.
(90) Inoue, K.; Ahmed, M.; Nihonyanagi, S.; Tahara, T. Effect of Hydrogen-Bond on Ultrafast Spectral Diffusion Dynamics of Water at Charged Monolayer Interfaces. *J. Chem. Phys.* **2019**, *150*, No. 054705.
(91) Cournia, Z.; Chatzigoulas, A. Allostery in Membrane Proteins. *Curr. Opin. Struct. Biol.* **2020**, *62*, 197−204.
(92) Sciacca, M. F. M.; Brender, J. R.; Lee, D.; Ramamoorthy, A. Phosphatidylethanolamine Enhances Amyloid Fiber Dependent Membrane Fragmentation. *Biophys. J.* **2012**, *102*, 488a.

https://dx.doi.org/10.1021/acs.jpcb.0c08755
J. Phys. Chem. B 2021, 125, 1343−1350